Real-Time Geometry-Based Cycle Slip Resolution Technique for Single-Frequency PPP and RTK

Sébastien CARCANAGUE, *ENAC/M3SYSTEMS, France*

BIOGRAPHY

Sébastien CARCANAGUE graduated as an electronic engineer in 2009 from the ENAC (Ecole Nationale de l'Aviation Civile) in Toulouse, France. Since 2009, he is a PhD student at the signal processing lab of ENAC and M3SYSTEMS working on precise positioning algorithm in constrained environments.

ABSTRACT

Raw carrier phase measurements from the Phase Lock Loop can be used to improve position accuracy. Techniques such as Real-Time Kinematic, Precise Point Positioning or code smoothing use the constancy of the ambiguity value over time to obtain a precise position. In the case of a cycle slip, these techniques have to be reinitialized which degrades the final quality of the solution. Although many techniques exist for dual-frequency data, single-frequency cycle slip resolution is still an open problem [Takasu, et al., 2008].

In this paper, a single-frequency ambiguity resolution technique based on Doppler measurements is presented. Instead of treating each satellite separately, the entire geometry is used to determine the cycle slip float solution. Moreover, an integer estimation technique is used to determine the integer cycle slip vector from the float solution. Tests will be conducted on real data from different environments showing improvements with regards to geometry-free technique.

Additionally, a new Doppler weighting scheme is introduced in the paper, taking into account both the speed of the vehicle and the carrier-to-noise density ratio.

1. INTRODUCTION

1.1 IMPROVING POSITIONING ACCURACY USING CARRIER-PHASE MEASUREMENTS

GPS receivers have become a device used by millions of drivers or pedestrians every day. Current positioning accuracy using code measurements is usually sufficient to lead the way of a car driver or a pedestrian into an unknown area. However, stand-alone positioning technique is not precise enough for a number of demanding applications: UAV's guidance systems, precise agriculture or mobile mapping systems are applications typically requiring decimeter or even centimeter accuracy, regardless of the environment.

To reach this level of accuracy, techniques using raw carrier phase measurements from the Phase Lock Loops (PLL) have been developed. Carrier phase measurements are more precise than code measurements by a factor of a hundred [Enge, et al., 2006]. However, they are ambiguous by an a priori unknown integer number of cycles called the ambiguity. This ambiguity remains constant as long as the PLL tracking is continuous.

Many techniques use the precision of the carrier phase to improve the accuracy of the final position. Some of them estimate the value of the ambiguity to turn carrier phase measurements into very precise absolute pseudoranges (Real-Time Kinematic and Precise Point Positioning). To do so, all biases affecting the carrier-phase measurements have to be removed by using precise ephemeris and parameter estimation (PPP) or by differencing with measurements coming from a spatially close reference station (RTK). Other techniques simply use the precise variation of the user-to-satellite range that can be obtained by differencing carrier phase measurements between 2 continuous epochs to smooth code measurements (Hatch filter [Hatch, 1982], position domain Hatch filter [Lee, et al., 2008]…). In both types of techniques, the constancy of the ambiguity value is used and in general the longer the time the ambiguity remains constant, the better the effect on the final position accuracy. However, the PLL can punctually create a variation of the ambiguity value by an integer number of cycles from an epoch to the other: it is called a cycle slip.

1.2 ORIGIN OF CYCLE SLIPS

A cycle slip is a discontinuity of the measured carrier phase resulting from a temporary loss of lock in the carrier tracking loop of a GNSS receiver [Kim, et al., 2002]. According to [Hofmann-Wellenhof, et al., 1997], there are 3 causes to cycle slips: signal obstruction, low signal-to-noise ratio and failure in the receiver software which leads to incorrect signal processing. A fourth cause pointed out by [Julien, 2005] is receiver dynamic implying a phase error within the integration time that is significantly higher than the PLL discriminator linear domain. Although usually relatively rare in static conditions, cycle slips occurrence can be very high for moving low-cost receivers [Realini, 2009]. It is then very important to detect them and if possible to repair them.

1.3 EFFECT OF CYCLE SLIPS ON SINGLE-FREQUENCY PRECISE POSITIONING TECHNIQUES

Undetected cycle slip can be very harmful to precise position algorithm as an uncontrolled error will propagate into the position estimation.

The effect of unrepaired cycle slips depends on the precise positioning algorithms. In the case of PPP and RTK, the estimated ambiguity has to be reinitialized after a detected cycle slip. It weakens the satellite geometry which usually results in a poorer position and a longer time to reach centimeter-level accuracy.

In the case of the Hatch filter, the cycle-slip-contaminated satellite smoothed pseudorange has to be reinitialized. Position domain smoothing is less affected by detected cycle slips and geometry changes [Lee, et al., 2008]. However, if the number of carrier phase measurements not affected by cycle slips drops below 4, the smoothing process also has to be reinitialized.

1.4 REAL-TIME SINGLE-FREQUENCY CYCLE SLIP DETECTION

As the detection of cycle slips is crucial for precise positioning software, many techniques have been developed for single-frequency users. They can be divided into 2 categories:

- **Statistical testing** ([Wang, 2003] and [Kamimura, et al., 2011]). Assuming a certain distribution of the carrier phase measurements residuals, the hypothesis "no cycle slip occurred" (null hypothesis) is tested versus the hypothesis " a cycle slip occurred" (alternative hypothesis). If the precise positioning algorithm uses a Kalman filter, the innovation of the Kalman filter can also be tested as in [Realini, 2009].
- **Phase prediction method.** The measured carrier phase is compared to the predicted carrier phase using Doppler measurements ([Wang, 2003]) and/or INS IMU sensors ([Lee, et al., 2003], [Takasu, et al., 2008]). If the difference between the two is over a certain threshold, the ambiguity is reinitialized to the float predicted value.

Although mandatory, cycle slip detection is usually not sufficient if cycle slips are very frequent. A major challenge is to repair them.

1.5 REAL-TIME SINGLE-FREQUENCY CYCLE SLIP RESOLUTION

Many techniques have been proposed for cycle slip resolution of dual-frequency GPS data ([Banville, et al., 2009], [Kim, et al., 2002], [Du, 2011],…). However, single-frequency cycle slip repair still seems to be an open problem in urban area, especially for a moving receiver [Takasu, et al., 2008]. In order to avoid the issue of cycle slip resolution, RTK with single-epoch ambiguity resolution is recommended for a moving receiver in difficult environments ([Bahrami, et al., 2010] and [Kubo, et al., 2008]) as it inherently avoids the issue of cycle slip amplitude estimation. However, single-epoch ambiguity resolution requires very precise code

measurements and is suboptimal as the constancy of the ambiguity value from one epoch to the other is not taken into account in the Kalman filter transition matrix. Indeed, cycle slips usually don't occur at every epoch on every satellite.

In this paper, a new real-time single-frequency cycle slip resolution technique is proposed. Contrary to techniques that treat each satellite separately, the technique estimates the amplitude of the cycle slip using the full geometry. Moreover, the full integer cycle slip vector is estimated using an ambiguity resolution technique. It will be shown that the integer cycle slip resolution technique directly benefits from velocity constraints that can be applied to a land vehicle and can be very easily implemented when both GPS and GLONASS measurements are used. Finally, a new weighting scheme will be proposed for Doppler measurements, taking into account both the speed of the vehicle and the carrier-to-noise density ratio.

2. PRESENTATION OF THE TECHNIQUE

2.1 OBSERVABLES MODEL

The relative motion of a satellite and the user results in changes in the observed frequency of the satellite signal [Enge, et al., 2006]. The Doppler measurement model for satellite i is:

$$D(k) \cdot \lambda_i = \dot{\rho}(k) + c\left(\dot{dt}(k) - \dot{dT}(k)\right) - \dot{I}(k) + \dot{T}(k) + \varepsilon \tag{1}$$

Where:

- $D(k)$ is the Doppler measurement in Hz at epoch k
- λ_i is satellite signal wavelength
- $\dot{\rho}(k)$ is the geometric range rate at epoch k
- $\dot{dt}(k)$ and $\dot{dT}(k)$ are the receiver and satellite clock bias rate respectively
- $\dot{I}(k)$ and $\dot{T}(k)$ are ionospheric and tropospheric delay rates.
- ε is Doppler unmodelled effects, including noise and multipath.

Carrier phase measurement model for satellite i is:

$$\phi^i(k) = \rho(k) + c(dt(k) - dT(k)) - I(k) + T(k) + b_{r,\phi}(k) - b_\phi^s(k) + N(k)\lambda_i + W(k)\lambda_i + \varepsilon_{\phi(k)} \tag{2}$$

Where:

- $\phi_i(k)$ is carrier phase measurement at epoch k
- $\rho(k)$ is the geometric range between satellite and receiver antenna,
- c is the speed of light,
- $dt(k)$ and $dT(k)$ are the biases associated to receiver and satellite oscillator offset
- $I(k)$ is the delay due to ionosphere
- $T(k)$ is the tropospheric delay,

- $b_{r,Obs}$ and b^s_{Obs} are the receiver and satellite hardware biases
- $W(k)$ is the wind-up effect error
- $\varepsilon_{\phi(k)}$ represents unmodelled errors of the observation
- $N(k)$ is the integer ambiguity value at epoch k

Then, using the mean Doppler between 2 epochs and differencing carrier phase measurement between 2 epochs and neglecting atmospheric delay, hardware delay, satellite clock and phase wind-up time differences, the following observables model can be obtained:

$$\begin{cases} \dfrac{D(k) + D(k-1)}{2} \cdot \lambda_i = \overline{\dot\rho} + c\overline{\dot{dt}} + \varepsilon_{\overline{D}} & (3a) \\ \phi^i(k) - \phi^i(k-1) = \delta\rho + c\delta dt + CS \cdot \lambda_i + \varepsilon_{\delta\phi} & (3b) \end{cases}$$

Where:

- $\overline{\dot\rho}$ and $\overline{\dot{dt}}$ are the average of 2 consecutive epochs range rate and clock bias rate respectively
- δ is the between epoch difference operator
- CS is the integer cycle slip

It can be seen that equation $(3a)$ is related to a velocity mean, whereas $(3b)$ is related to a range difference. However, if the 2 consecutive epochs are close enough in time so that the acceleration and the clock bias jerk can be considered constant on the interval:

$$\overline{\dot\rho} \approx \frac{\delta\rho}{\Delta t} \text{ and } \overline{\dot{dt}} \approx \frac{\delta dt}{\Delta t}$$

where $\Delta t = t(k) - t(k-1)$ and $t(k)$ and $t(k-1)$ are the measurement time at epoch k and $k-1$. In practice, a data rate of 1 Hz was found to be sufficient in the case of a land vehicle and a low-cost receiver clock.

Therefore, the final observable model for a high data rate receiver is:

$$\begin{cases} \dfrac{D(k) + D(k-1)}{2} \cdot \lambda_i \cdot \Delta t = \delta\rho + c\delta dt + \varepsilon_{\frac{\delta D}{2} \cdot \Delta t} & (4a) \\ \phi^i(k) - \phi^i(k-1) = \delta\rho + c\delta dt + CS \cdot \lambda_i + \varepsilon_{\delta\phi} & (4b) \end{cases}$$

The condition on the clock bias rate might be the most difficult to meet especially on a receiver with frequent clock adjustments. In order to avoid this issue, between-satellite differences can be made to eliminate the clock term if GPS-only measurements are used. However, it can be a problem if GLONASS measurements are used as undifferenced float cycle slip vector has to be estimated, as explained in 3.1.

To correct for the satellite contribution in the geometric range change, corrections are applied to the 2 observables, following [van Graas, et al., 2003]. The final matrix form, linking observables to position time variation is:

$$Y = H \begin{bmatrix} \delta X \\ \delta dt \end{bmatrix} + \begin{bmatrix} 0 \\ CS \cdot \lambda \end{bmatrix} + \varepsilon \qquad (5)$$

where:

- $Y = \begin{bmatrix} \vdots \\ \dfrac{D^i(k) + D^i(k-1)}{2} \cdot \lambda_i \cdot \Delta t \\ \vdots \\ \phi^i(k) - \phi^i(k-1) \\ \vdots \end{bmatrix} - correction$ where

  $correction$ is the satellite contribution in the geometric range change, as well as modeled tropospheric delay variation and satellite clock change obtained from broadcast ephemeris (see Appendix 0).
- δX is the time variation of the position.
- CS is the integer cycle slip vector and λ is the satellite wavelength vector.

It can be seen that we obtain 2 types of observables: a precise but ambiguous observable derived from carrier phase measurements and an unambiguous but coarse observable derived from Doppler measurements.

Then, cycle slip can be repaired using integer vector estimation techniques similarly to ambiguity resolution in the position domain. After integer cycle slip estimation, a residual test is performed to validate the integer vector. In the case that the integer cycle slip vector is rejected, cycle slip vector is kept as a float and velocity is derived from Doppler measurements. A scheme of the algorithm can be found on Figure 1. The processing is very similar to ambiguity resolution in the position domain, with different observables. One difference is that cycle slip estimation has to be performed in a single-epoch by definition. This condition is usually difficult to meet for ambiguity resolution. However, in the case of cycle slip resolution, the unambiguous observable based on mean Doppler value is significantly more accurate than code measurements. Moreover, estimating velocity together with cycle slip vector presents a certain number of advantages as described in the next section.
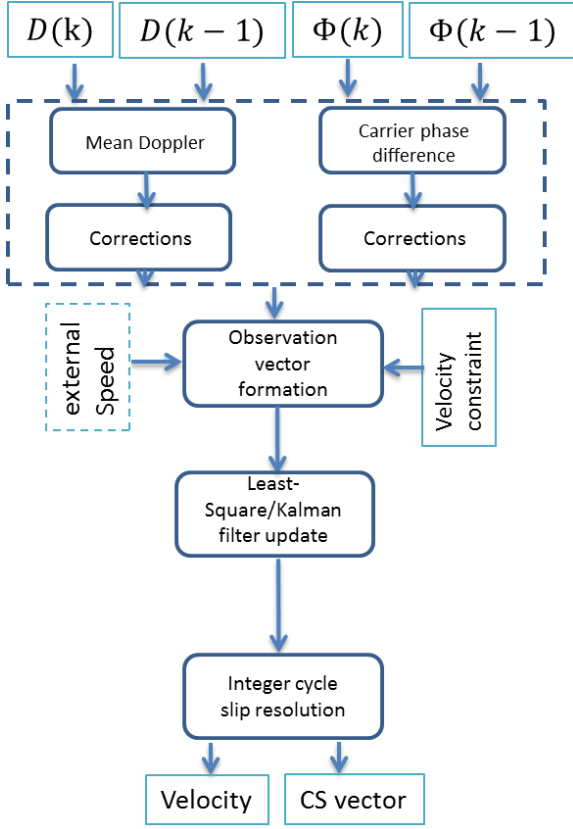
Figure 1 Scheme of the cycle slip resolution algorithm

2.2 POTENTIAL ADVANTAGES OF THE TECHNIQUE

In the presented technique, a complete filter is dedicated to cycle slip resolution estimating position variation and clock variation together with integer cycle slip vector.

The first advantage of such a scheme is that the float solution of the cycle slip vector benefits from the entire geometry.

A second advantage is that contrary to phase prediction method using Doppler and INS as in [Takasu, et al., 2008] or [Du, 2011], the covariance of the float cycle slip vector is a direct by-product of the estimation. It allows an optimal estimation of the closest integer vector, taking into account the covariance matrix of the float cycle slips vector.

Moreover, speedometers and inertial measurements units provides external estimation of the speed. This information can directly improve the solution by constraining both the float solution and the integer estimation. In the case of a land vehicle, vertical constraint can also be easily applied.

Additionally the presented technique relies on time-differenced carrier phase measurements, which are less affected by time correlated error such as static multipath. Integer estimation techniques being heavily influenced by carrier phase residuals, the cycle slip can potentially be easier to estimate than the ambiguity in 1 epoch using single-epoch RTK.

Finally, as detailed in the next sub-section, GLONASS measurements can easily be included together with GPS measurements to estimate a full multi-constellation integer cycle slip vector.

3. IMPLEMENTATION

3.1 GLONASS MEASUREMENTS INTEGRATION

Unlike GPS or GALILEO, which transmit in using CDMA (each satellite transmit a different PRN on a common frequency), GLONASS employs Frequency Division Multiple Access (FDMA) and transmits a common PRN on different frequencies [Enge, et al., 2006]. GLONASS satellite carrier phase model for satellite i is [Rossbach, 2000]:

$$\phi^i = \rho + c(dt - dT) - I^i + T + b_{r,\phi_i} - b^s_{r,\phi_i} + N\lambda^i + \varepsilon_{\phi^i}$$

Where:
- λ^i is the signal frequency depending on broadcasting satellite
- b^s_{r,ϕ_i} is an inter-channel bias depending on both the receiver and the satellite.

It implies 2 things for GLONASS ambiguity resolution [Ong, 2010]:
- The presence of inter-channel biases results in a bias $b^s_{r,\phi^i-\phi^k}$ on the measurement that is both satellite and receiver dependent, preventing the ambiguity from being estimated as an integer.
- The wavelength of the carrier is different on each satellite. When performing between satellite differences, an additional ambiguity has to be estimated:

$$\phi^i - \phi^{ref} = (\rho^i - \rho^{ref}) + c(dT^i - dT^{ref}) - I^i + I^{ref} + T^i - T^{ref} - b^s_{r,\phi^i-\phi^{ref}} + (N^i - N^{ref})\lambda^i + \underbrace{N^{ref}}_{\substack{additional \\ ambiguity}}(\lambda^i - \lambda^{ref}) + \varepsilon_{\phi^i-\phi^k}$$

The maximum wavelength value of the additional ambiguity is $(\lambda^i - \lambda^k) = 0.85mm$

However, the time-variation of the inter-channel bias can be neglected for a very short interval.

In order to cope with the different wavelengths of GLONASS measurements, integer cycle slip resolution is performed in 4 steps:
- Undifferenced cycle slip vector is estimated. Observation model from equation (5) is used.
- A reference satellite is chosen and between-satellite differences are performed. Carrier phase observation vector is corrected from additional ambiguity and a new adjustment is performed to determine integer single-differenced ambiguity vector using LAMBDA method.
- In order to obtain an undifferenced cycle slip vector, the reference satellite cycle slip value is set to zero.
- Reference satellite undifferenced cycle slip value from first step is added to the cycle slip vector.

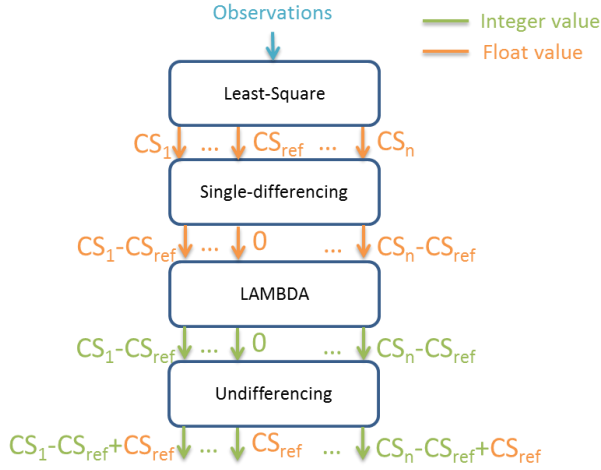A scheme of the cycle slip vector construction can be found on Figure 2.

Figure 2 Scheme of the cycle slip vector construction

Figure 3 Ratio of the vertical speed to the total speed norm for 15 sessions of approximatively 1 hour in Bordeaux and Nantes. Mean = 0.04% and σ= 2.1% .Epochs with a speed norm inferior to 20cm.s^{-1} have been rejected.

If the last step is omitted, the cycle slip vector depends on the reference satellite chosen. Indeed, in the case of GPS measurements, an arbitrary amount of cycles can be added to the cycle slip vector, as it will be absorbed in the common clock bias. In the case of GLONASS, adding a random number of cycles to the cycle slip vector impact satellites differently as the wavelengths are different. The cycle slip vector can then be used in a RTK or PPP software, regardless of the reference satellite chosen.

GLONASS satellite measurements were implemented as so in the software. An additional advantage is that although the absolute value of the receiver clock bias relative to GPS Time and GLONASS Time is different, the clock bias rate is the same as it is derived from the same oscillator. A unique clock bias rate parameter was estimated in the software for both GPS and GLONASS satellites.

3.2 VELOCITY CONSTRAINT

As the technique was intended to be used with a land vehicle, a vertical velocity constraint was applied. A virtual velocity observation, null in the up direction, was added to the observation vector. To determine the error statistic associated to this observation, velocity data collected during a measurement campaign on different French roads near Nantes and Bordeaux was analyzed. The ratio of the vertical speed over the absolute 3D velocity is plotted on Figure 3. Epochs with a speed norm inferior to 20cm.s^{-1} were rejected. Indeed the vertical speed is then close to a centimeter/second and the reference velocity was not accurate enough to conclude on such low speed data.
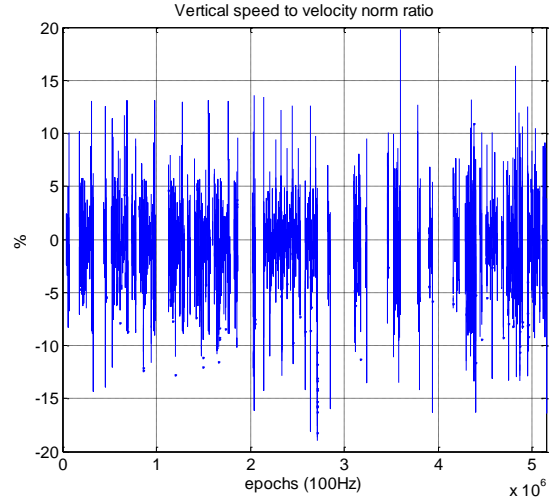
The standard deviation of the ratio of the vertical speed to the total speed norm was found to be 2.1%.

The sigma associated to the null vertical speed observation was then set to $\sigma = 0.02 * \|speed\|$ where $speed$ is the velocity estimated at the previous epoch.

## 4. DOPPLER WEIGHTING

4.1 DOPPLER MULTIPATH ANALYSIS

Doppler measurements are relatively difficult to weight. Indeed, [Aminian, 2011] underlines that multipath effect on Doppler measurements depends on both signal-to-noise ratio and velocity. In a static environment, influence of multipath signals on Doppler measurements is null, as the frequency of the reflected signals and the direct signal are equal. Then measurements can be weighted using FLL tracking loop jitter due to thermal noise, as in [Kubo, 2009] or [Aminian, 2011]. However this weighting would be overly optimistic in the case of a moving antenna.

In order to illustrate this, data from a Novatel DLV3 receiver and a uBlox LEA-4T connected to a Novatel geodetic-grade antenna was analyzed. The Novatel receiver data rate was 1Hz whereas the uBlox receiver data rate was 4Hz. The antenna was mounted on the top of a car, during 8 sessions of approximately 1 hour each. Data was collected on May 4th and 5th, 2009. During 4 sessions, the car was driven on rural roads near Biscarosse, France. For the remaining 4 sessions, the car was driven on Bordeaux's beltway under normal traffic conditions. The maximum speed was around 90km/h for all sessions. The reference speed and trajectory were post-processed using dual-frequency GPS/GLONASS data and a tactical grade IMU. Doppler multipaths were isolated, removing the satellite velocity contribution using broadcast ephemeris and receiver velocity from the post-processed reference velocity. Between-satellite differences were formed to eliminate the clock rate term. The satellite with the highest C/N$_0$ was chosen as

reference satellite. Results can be found on Figure 4 and Figure 5.

Doppler Single-differenced (between satellite) residuals versus Reference velocity norm
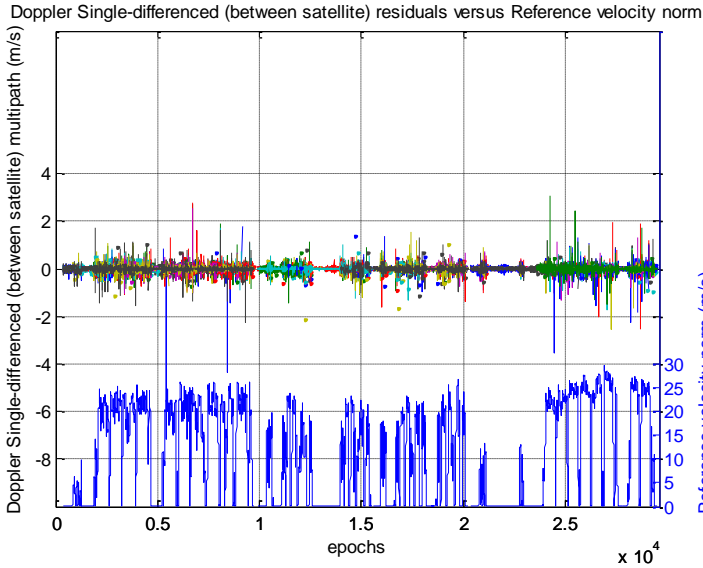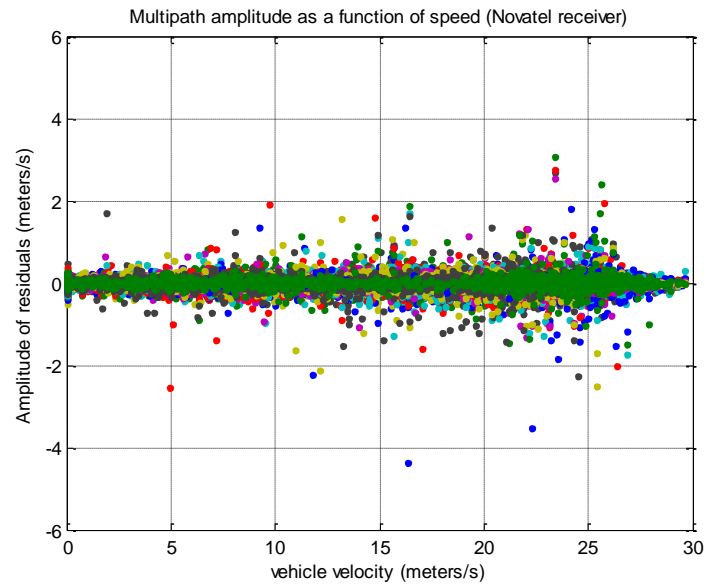

Figure 4 Single-differenced Doppler multipath and receiver velocity (Novatel receiver, 1Hz data collected on rural roads near Biscarosse and on Bordeaux's beltway, France)
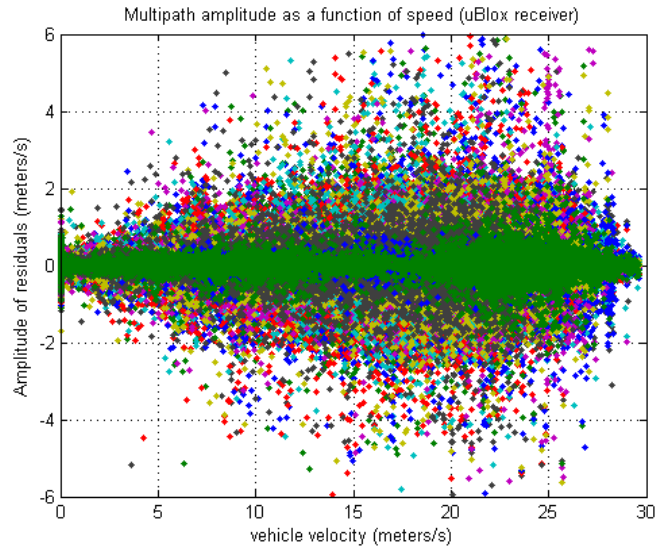
Doppler Single-differenced (between satellite) residuals versus Reference velocity norm
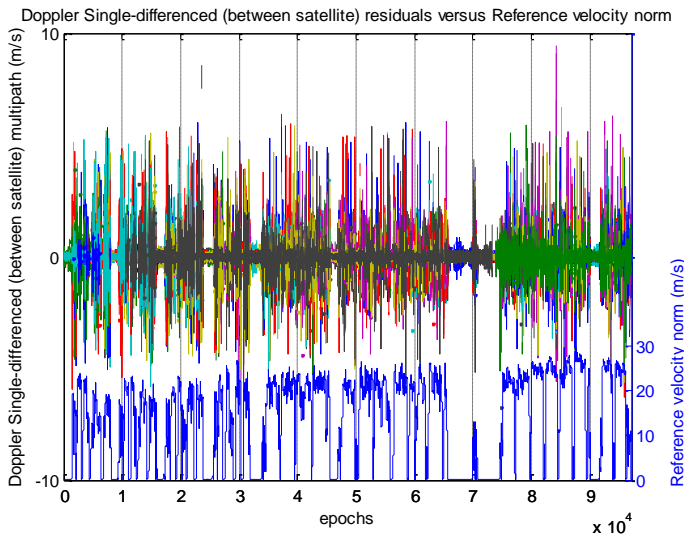
Figure 5 Doppler single-differenced multipath versus receiver velocity (uBlox receiver, 4Hz data collected on rural roads near Biscarosse and on Bordeaux's beltway, France)

As expected, multipath residuals are heavily correlated with the vehicle speed.

In order to determine a link between vehicle speed and multipath amplitude, multipath residuals were plotted as a function of the vehicle velocity norm. Results can be found on Figure 6 and Figure 7 for Novatel and uBlox receiver respectively.

Multipath amplitude as a function of speed (Novatel receiver)

Figure 6 Doppler single-differenced multipath as a function of receiver velocity (Novatel receiver, 1Hz data collected on rural roads near Biscarosse and on Bordeaux's beltway, France)

Multipath amplitude as a function of speed (uBlox receiver)

Figure 7 Doppler single-differenced multipath as a function of receiver velocity (uBlox receiver, 4Hz data collected on rural roads near Biscarosse and on Bordeaux's beltway, France)

In the case of the uBlox receiver, multipath tends to increase with the vehicle speed until a speed around 15m/s, and decrease after this value.
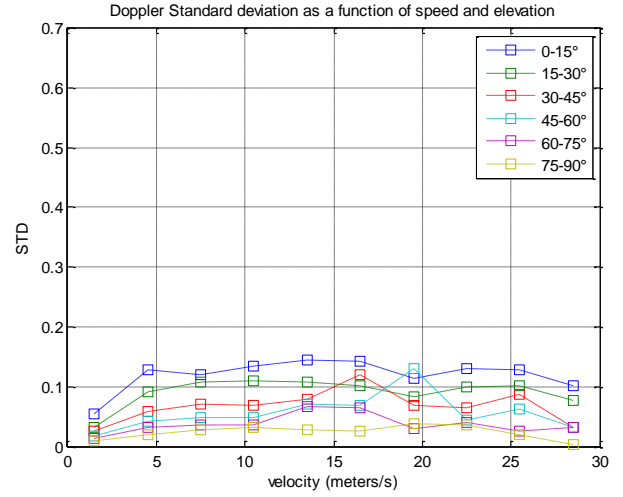
An interpretation is that the vehicle speed increases the frequency of the multipath. If the variation of the phase (or frequency) of the multipath exceeds the PLL (or FLL) bandwidth, the multipath effects on tracking starts to be filtered out. In the case of the high-end receiver, Doppler multipath is heavily reduced and seems relatively stable with speed.

In order to determine the influence of both speed and C/N_0 on Doppler measurements, the standard deviation of the Doppler measurements was estimated as a function of the vehicle speed and C/N_0, as seen on Figure 8 and Figure 9.
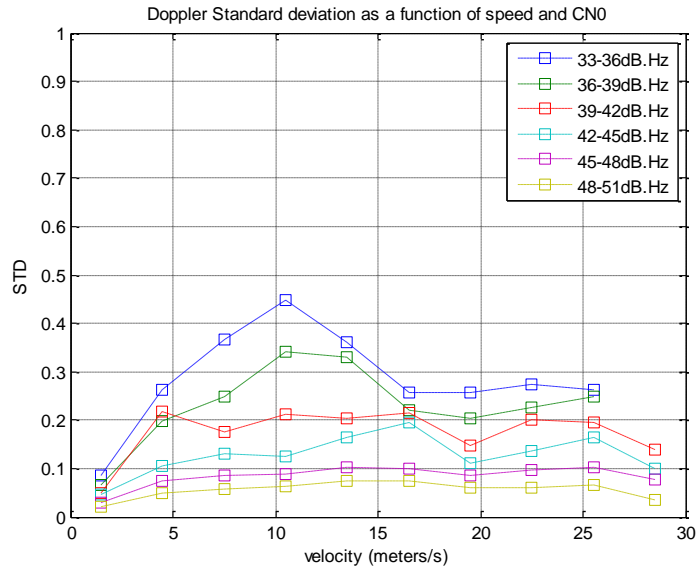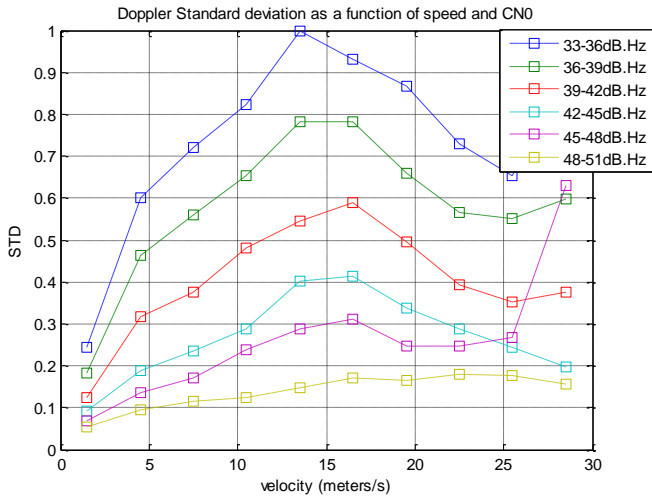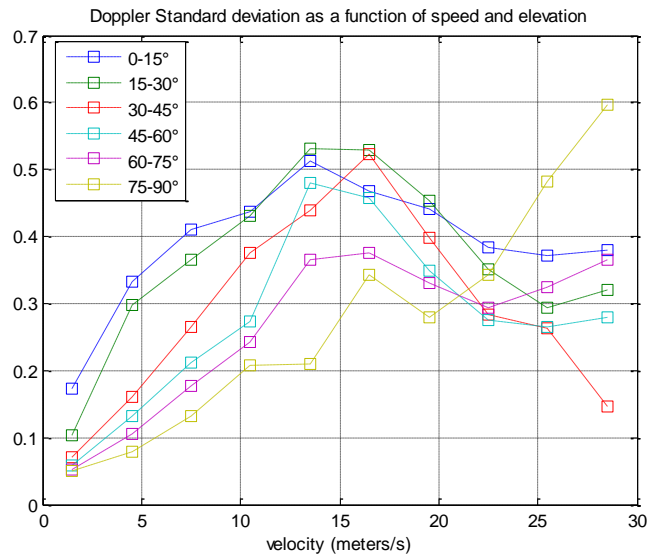
Figure 8 Estimated standard deviation of Doppler multipath on Novatel receiver (1Hz data), as a function of speed and C/N$_0$. Standard deviation was estimated for speed "slices" of 3m.s^{-1}, from 0 to 30 m.s^{-1}

Figure 9 Estimated standard deviation of Doppler multipath on uBlox receiver (4Hz data), as a function of speed and C/N0. Standard deviation was estimated for speed "slices" of 3m.s^{-1}, from 0 to 30 m.s^{-1}

A clear trend is visible for both receivers. The maximum standard deviation value is obtained around 15 m.s^{-1} for the Novatel receiver and around 10 to 15 m.s^{-1} for the uBlox. This is likely due to different carrier tracking strategies between the 2 receivers. Another interesting point is that the Novatel receiver provides Doppler measurements that are about twice more precise than the uBlox receiver.

A second parameter often used for weighting GNSS measurements is the satellite elevation. In order to determine if the satellite elevation is a relevant parameter to weight Doppler measurements of a moving receiver, the Doppler error standard deviation is plotted as a function of speed and satellite elevation. Results can be found on Figure 10 and Figure 11.

Figure 10 Estimated standard deviation of Doppler multipath on Novatel receiver (1Hz data), as a function of speed and elevation. Standard deviation was estimated for speed "slices" of 3m.s^{-1}, from 0 to 30 m.s^{-1}

Figure 11 Estimated standard deviation of Doppler multipath on uBlox receiver (4Hz data), as a function of speed and elevation. Standard deviation was estimated for speed "slices" of 3m.s^{-1}, from 0 to 30 m.s^{-1}

Although a trend also exists with elevation, the C/N$_0$ value seems to better characterize the Doppler error STD from different satellites.

As a result, a weighting that takes into account both the vehicle speed and the Carrier-to-Noise density ratio was chosen.

4.2 PROPOSED DOPPLER WEIGHTING SCHEME

In order to weight measurements using both vehicle speed and C/N$_0$, a new weighting scheme is proposed based on a look-up table. The tables for a Novatel DLV3 receiver, a uBlox LEA-4T connected to a geodetic antenna can be found on Table 1 and Table 2.

Doppler measurements are weighted using the standard deviation value of the matching table box. Values in the

table are derived from Figure 8 and Figure 9. Although they were not discussed in the previous section for sake of conciseness, standard deviation values for a uBlox LEA-4T connected to a patch antenna are also given in Table 3. Related plots can be found in Appendix B.

Table 1 Doppler multipath standard deviation values in m.s^{-1}, as a function of receiver speed and C/N$_0$ for a Novatel DLV3 connected to a geodetic antenna.

Novatel DLV3 + Geodetic antenna

Vehicle speed	C/N$_0$					
	33-36 dB.Hz	36-39 dB.Hz	39-42 dB.Hz	42-45 dB.Hz	45-48 dB.Hz	48-51 dB.Hz
0 - 3 m.s^{-1}	0,09	0,07	0,05	0,05	0,03	0,02
3 - 6 m.s^{-1}	0,26	0,20	0,22	0,10	0,08	0,05
6 - 9 m.s^{-1}	0,37	0,25	0,17	0,13	0,09	0,06
9 - 12 m.s^{-1}	0,45	0,34	0,21	0,13	0,09	0,06
12 - 15 m.s^{-1}	0,34	0,33	0,20	0,16	0,10	0,07
15 - 18 m.s^{-1}	0,26	0,22	0,21	0,19	0,10	0,07
18 - 21 m.s^{-1}	0,26	0,20	0,15	0,11	0,09	0,06
21 - 24 m.s^{-1}	0,27	0,23	0,20	0,13	0,10	0,06
24 - 27 m.s^{-1}	0,26	0,25	0,20	0,17	0,10	0,07
27 - 30 m.s^{-1}	-	-	0,14	0,10	0,08	0,03

Table 2 Doppler multipath standard deviation values in m.s^{-1}, as a function of receiver speed and C/N$_0$ for a uBlox LEA-4T connected to a geodetic antenna.

uBlox LEA-4T + Geodetic antenna

Vehicle speed	C/N$_0$					
	33-36 dB.Hz	36-39 dB.Hz	39-42 dB.Hz	42-45 dB.Hz	45-48 dB.Hz	48-51 dB.Hz
0 - 3 m.s^{-1}	0,24	0,18	0,13	0,09	0,07	0,05
3 - 6 m.s^{-1}	0,60	0,46	0,32	0,19	0,13	0,10
6 - 9 m.s^{-1}	0,72	0,56	0,38	0,24	0,17	0,12
9 - 12 m.s^{-1}	0,82	0,65	0,48	0,29	0,24	0,12
12 - 15 m.s^{-1}	1,00	0,78	0,55	0,40	0,29	0,15
15 - 18 m.s^{-1}	0,93	0,78	0,59	0,41	0,31	0,17
18 - 21 m.s^{-1}	0,87	0,66	0,50	0,34	0,25	0,17
21 - 24 m.s^{-1}	0,73	0,57	0,39	0,29	0,25	0,18
24 - 27 m.s^{-1}	0,65	0,55	0,35	0,24	0,27	0,18
27 - 30 m.s^{-1}	0,87	0,60	0,37	0,20	0,63	0,16

Table 3 Doppler multipath standard deviation values in m.s^{-1}, as a function of receiver speed and C/N$_0$ for a uBlox LEA-4T connected to a geodetic antenna

uBlox LEA-4T + patch antenna

Vehicle speed	C/N$_0$					
	33-36 dB.Hz	36-39 dB.Hz	39-42 dB.Hz	42-45 dB.Hz	45-48 dB.Hz	48-51 dB.Hz
0 - 3 m.s^{-1}	0,26	0,20	0,14	0,10	0,08	0,05
3 - 6 m.s^{-1}	1,05	0,71	0,41	0,27	0,19	0,10
6 - 9 m.s^{-1}	1,09	0,77	0,54	0,35	0,22	0,11
9 - 12 m.s^{-1}	1,46	0,77	0,56	0,43	0,25	0,10
12 - 15 m.s^{-1}	1,62	1,06	0,82	0,49	0,25	0,11
15 - 18 m.s^{-1}	1,18	1,06	0,85	0,53	0,27	0,11
18 - 21 m.s^{-1}	1,34	0,77	0,56	0,42	0,24	0,09
21 - 24 m.s^{-1}	1,26	1,14	0,75	0,35	0,25	0,10
24 - 27 m.s^{-1}	0,81	0,58	0,44	0,31	0,25	0,08
27 - 30 m.s^{-1}	0,90	0,61	0,51	0,30	0,31	0,09

5. CYCLE SLIP RESOLUTION TEST ON REAL DATA

5.1 RURAL ROAD NEAR NANTES

The cycle slip resolution algorithm was first tested using a data set collected in Nantes, France by a GPS/GLONASS Novatel DLV3 receiver mounted on the top of a car on April 29th, 2009. Only GPS/GLONASS L1 measurements were used. A maximum of 5 GLONASS satellites were visible at the same time during the session. The car alternated static and dynamic motion on rural roads with a good satellite visibility. Maximum speed was 10 meters.s^{-1}. The trajectory is plotted in yellow on Figure 12.
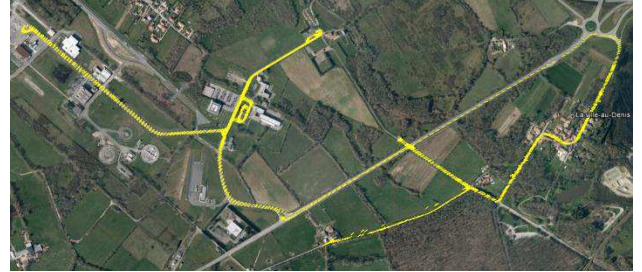
Figure 12 Trajectory of the car near Nantes, France ©2012 Google

Doppler measurements were weighted using the look-up Table 1. If the number of visible satellite dropped below 5, cycle slip vector was kept as a float.

To test the efficiency of the technique, a random integer cycle slip vector was added to GPS/GLONASS carrier phase measurements at each epoch, on every satellite, after that initial cycle slips were removed from data using dual-frequency analysis. Three cycle slip estimation methods are tested in the following. The first method, considered as the reference method, is to simply difference mean Doppler and time-differenced carrier phase measurements on each satellite (geometry-free method). The second method is to estimate the float value of the cycle slip vector with a least-square adjustment using equation (4a) and (4b) (geometry-based method). The third method is to apply an additional integer estimation technique (LAMBDA method [Teunissen P. , 1993]) to determine the integer cycle slip (geometry-based+integer estimation method). Each time, between-satellite differenced estimated cycle slip vectors were compared to between-satellite differenced true cycle slip vector, because estimated vector could differ from true cycle slip vector by an integer number of wavelength absorbed by the estimated clock. Geometry-free and geometry-based method residuals can be found on Figure 13 and Figure 14.
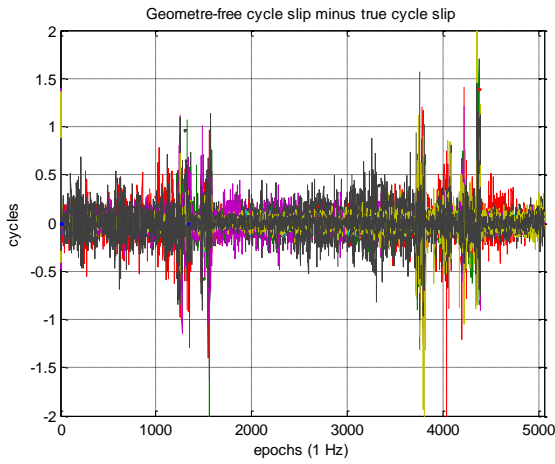
Figure 13 Estimated cycle slip vector minus true cycle slip vector using geometry-free method in Nantes, on April 29th, 2009 with a Novatel DLV3 receiver.
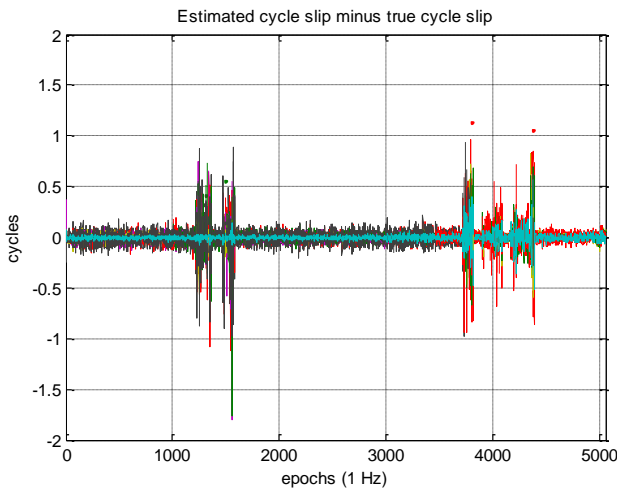

Figure 14 Estimated cycle slip vector minus true cycle slip vector using geometry-based technique in Nantes, on April 29th, 2009 with a Novatel DLV3 receiver.

Epochs when the vehicle is in motion are clearly visible on Figure 14, as multipath effect is higher. It can be seen that the accuracy of the geometry-free and geometry based method is not sufficient to determine the cycle slip vector with a simple rounding, especially when the receiver is in motion. The results of the geometry-based+integer estimation method can be found on Table 4.

Table 4 Cycle slip resolution success rate in Nantes

	Nantes
Number of epochs (1Hz)	5052
Percentage of epochs with at least 5 time-differenced carrier phase measurements available (GPS/GLONASS)	99.1%
Percentage of epochs with integer cycle slip correctly resolved	97.9%

Time-differenced carrier phase measurements availability statistic is given, as it is an important part of the proposed method fail rate. Although adding cycle slips on every satellite at each epoch is a very challenging scenario, the proposed method has a very high success rate.

5.2 URBAN AND SEMI-URBAN ENVIRONMENT IN TOULOUSE WITH A LOW-COST RECEIVER

In order to test the technique with a more difficult environment and a low-cost receiver, a data collection was performed on July 3rd, 2012. The test used a NVS-08C, which is a low-cost (chip is less than 40 euros) receiver tracking L1 GPS/GLONASS signals. The receiver was connected to patch antenna from Tallysman Wireless. Trajectory can be found on Figure 15. The urban environment can be considered as very difficult, as the vehicle went through narrow streets of the old downtown. Moreover, frequent signal outages were noticed on the beltway due to bridge crossing.
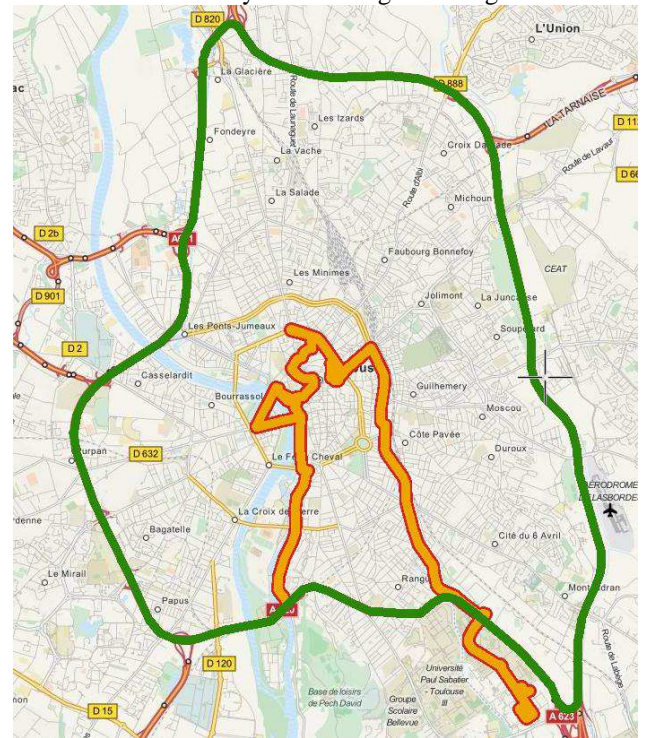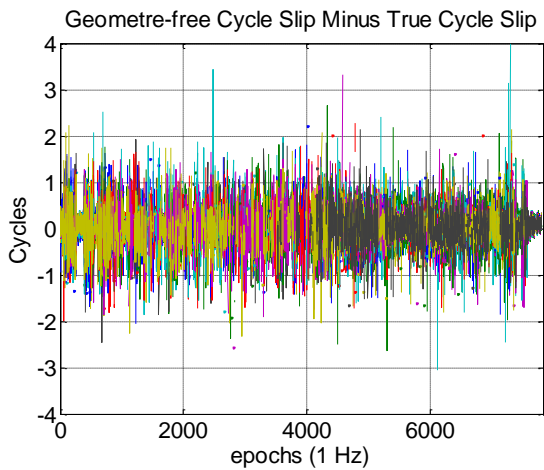

Figure 15 Trajectory of the car on Toulouse's beltway (in green) and in downtown Toulouse (in orange) © OpenStreetMap contributors

Similarly to the first experiment, cycle slips were first monitored and removed from the data set. Then a random cycle slip (integer from -100 to 100) is added at each epoch on each satellite.

The geometre-free method residuals can be found on .

Figure 16 Estimated cycle slip vector minus true cycle slip vector using geometry-free technique in Toulouse, on July 3rd, 2012 with a NVS-O8C connected to a patch antenna.

It can be seen that with such a low-cost receiver in difficult environment, cycle slip repair is simply impossible due to the low accuracy of Doppler measurements.

Cycle slip resolution success rate in both environments is summarized in Table 5. To obtain these results, Doppler measurements of the NVS receiver were weighted using Table 3. Indeed, data set collected was not sufficient to derive a table with sufficient confidence. However, Doppler multipath estimated standard deviation was found to have a very similar vehicle speed and C/N_0 value dependency as the uBlox LEA-4T equipped with a patch antenna.

Table 5 Bordeaux's beltway cycle slip resolution success rate

	Toulouse beltway (low-cost receiver)		Downtown Toulouse (low-cost receiver)	
Number of epochs	2712		4510	
	GPS-only (1Hz)	GPS+ GLONASS (1Hz)	GPS-only (1Hz)	GPS+ GLONASS (1Hz)
Percentage of availability (at least 5 time-differenced carrier phase measurements visible)	70.6%	78.9%	43.9%	66.5%
Percentage of epochs with cycle slip resolved as integer	64.4%	73.4%	34.9%	54.3%

As expected, the success rate is lower with a low-cost receiver in such difficult environments than on rural roads with a high end receiver. It is certainly due to multipath on carrier phase and Doppler measurements, as well as worst satellite visibility. The availability of time-differenced carrier phase measurement is an important factor of failure of the algorithm, as seen on the first line of Table 5. Lastly the improvement brought by GLONASS in term of carrier phase measurements availability is also very clear in both environments.

However, despite the addition of cycle slips at each epoch and the low cost of the positioning module, the ambiguity could be estimated continuously with a RTK/PPP software more than 50% of the time in urban environment and almost 75% of the time on the beltway thanks to the proposed technique.

6. CONCLUSION

In this paper, a real-time single frequency cycle-slip resolution technique is introduced. Compared to algorithms processing each satellite separately, the technique uses the entire geometry and potentially additional speed sensors to determine the amplitude of the cycle slip. Moreover, it uses integer estimation theory (LAMBDA method) to estimate the integer cycle slip vector from the float vector. The cycle slip resolution technique is very easily implementable with different constellation as a unique clock bias rate is estimated.

Moreover, a new Doppler weighting scheme based on both receiver speed and observable C/N_0 is introduced in the paper. Standard deviation values are given for a geodetic-grade receiver and a low-cost high-sensitivity receiver.

The cycle slip ambiguity resolution technique and the Doppler weighting scheme were tested on 2 data sets. In all cases, geometry-based technique gave better accuracy than geometry-free technique, even when integer cycle-slip validation failed and cycle slip value was kept as float.

However, improvement on the position domain and on carrier phase ambiguity estimation brought by the proposed cycle slip resolution technique was not tested. Moreover, only 1 Hz data rate was tested. Impact of lower data rate has to be investigated.

REFERENCES

Aminian, B. (2011). *Investigation of GPS Observations for Indoor GPS/INS Integration.* Master of Science thesis, Department of Geomatics Engineering, University of Calgary, Alberta.

Bahrami, M., & Ziebart, M. (2010). *Instantaneous Doppler-Aided RTK Positioning with Single Frequency Receivers.* Proceedings of IEEE/ION Position Location and Navigation Symposium (PLANS).

Banville, S., & Langley, R. B. (2009). *Improving Real-Time Kinematic PPP with Instantaneous Cycle-Slip Correction.* ION GNSS: 22nd International Meeting of the Satellite Division of The Institute of Navigation, Savannah, GA, September 22-25, 2009.

Du, S. (2011). *An Inertial Aided Cycle Slip Detection and Identification Method for Integrated PPP GPS/MEMS IMU System.* 24th International Technical Meeting of the Satellite Division of the Institute of Navigation, Portland, OR, September 19-23.

Enge, P., & Misra, P. (2006). *GLOBAL POSITIONING SYSTEM Signals, Measurements, and Performance.* Ganga-Jamuna Press, 2nd Edition.

Hatch, R. (1982). *The synergism of GPS code and carrier measurements.* New Mexico: Proceedings of the Third International Geodetic Symposium on Satellite Doppler Positioning.
Hofmann-Wellenhof, B., Lichtenegger, H., & Collins, J. (1997). *GPS Theory and Practice.* 4th Edition, Springer-Verlag, Wien.

Julien, O. (2005). *Design of Galileo L1F Receiver Tracking Loops. PhD Thesis, published as UCGE Report No. 20227, Department of Geomatics Engineering, The University of Calgary.*

Kamimura, K., Tomita, R., Nagano, T., Chabata, A., Kubo, Y., & Sugimoto, S. (2011). *Detection of Cycle Slips and Multipath in GNSS RTK Precise Point Positioning.* 24th International Technical Meeting of the Satellite Division of the Institute of Navigation, Portland, OR, September 19-23.

Kim, D., & Langley, R. B. (2002). *Instantaneous Real-Time Cycle-Slip Correction for Quality Control of GPS Carrier-Phase Measurements.* Navigation/ Department of Geodesy and Geomatics Engineering, UNB.

Kubo, N. (2009). *Advantage of velocity measurements on instantaneous RTK positioning.* GPS Solutions, vol. 13, 2009, pp. 271-280.

Kubo, N., & Pullen, S. (2008). *Instantaneous RTK Positioning Based on User Velocity Measurements.* ION GNSS 21st International Technical Meeting of the Satellite Division, 16-19, September 2008, Savannah, GA.

Leandro, R., Santos, M., & Langley, R. B. (2006). *UNB Neutral Atmosphere Models: Development and Performance.* ION NTM 2006,18-20 January 2006, Monterey, CA.

Lee, H. K., & Rizos, C. (2008). *Performance Analysis of Position-Domain Hatch filter.* IEEE TRANSACTIONS ON AEROSPACE AND ELECTRONIC SYSTEMS VOL. 44, NO. 1.

Lee, H.-K., Wang, J., & Rizos, C. (2003). *Carrier Phase Processing Issues for High Accuracy Integrated GPS/Pseudolite/INS Systems.* Proceedings of 11th IAIN World Congress, Berlin, Germany, paper 252.

Ong, R. (2010). *Reliability of combined GPS/GLONASS Ambiguity resolution.* Master of Science thesis, Department of Geomatics Engineering, University of Calgary, Alberta.

Realini, E. (2009). *goGPS free and constrained relative kinematic positioning with low cost receivers.* PhD thesis, Politecnico Di Milano.

Rossbach, U. (2000). *Position and Navigation Using the Russian Satellite System GLONASS.* University FAF Munich, Faculty of civil and Surveying Engineering, Germany.

Takasu, T., & Yasuda, A. (2008). *Cycle Slip Detection and Fixing by MEMS-IMU/GPS Integration for Mobile Environment RTK-GPS.* ION GNSS 21st International Technical Meeting of the Satellite Division, 16-19, September 2008, Savannah, GA.

Teunissen, P. (1993). *Least-squares estimation of the integer GPS ambiguities.* Invited lecture, Section IV Theory and Methodology, IAG General Meeting, Beijing, China, August.

van Graas, F., & Soloviev, A. (2003). *Precise Velocity Estimation Using a Stand-Alone GPS Receiver.* ION NTM 2003, 22-24 January 2003, Anaheim, CA.

Wang, C. (2003). *Development of a Low-cost GPS-based Attitude Determination System.* Master of Science thesis, Department of Geomatics Engineering, University of Calgary, Alberta.

A. APPENDIX: LINKING TIME-DIFFERENCED GEOMETRIC RANGE TO TIME-DIFFERENCED POSITION

Following [van Graas, et al., 2003], the time-differenced geometric range can be expressed as such:

$$\delta\rho = \rho(t_2) - \rho(t_1)$$
$$= \boldsymbol{e}(t_2).[\boldsymbol{SV}(t_2) - \boldsymbol{b}(t_2)] - \boldsymbol{e}(t_1).[\boldsymbol{SV}(t_1) - \boldsymbol{b}(t_1)]$$

Where:

- $\boldsymbol{e}(t_i)$ is the user to satellite line-of-sight vector at time t_i
- $\boldsymbol{SV}(t_i)$ is the satellite position vector in the ECEF reference frame at time t_i
- $\boldsymbol{b}(t_i)$ is the user position vector at time t_i
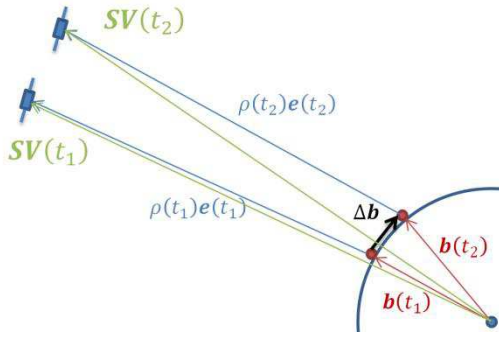
Notations are summarized on Figure 17.

Figure 17 Time-differenced model geometry

Expressing $\delta\rho$ as a function of $\Delta\boldsymbol{b} = \boldsymbol{b}(t_2) - \boldsymbol{b}(t_1)$:

$$\delta\rho = \boldsymbol{e}(t_2).\left[\boldsymbol{SV}(t_2) - \boldsymbol{b}(t_2)\right] - \boldsymbol{e}(t_1).\left[\boldsymbol{SV}(t_1) - \boldsymbol{b}(t_1)\right]$$

$$= \boldsymbol{e}(t_2)\boldsymbol{SV}(t_2) - \boldsymbol{e}(t_1)\boldsymbol{SV}(t_1) - \boldsymbol{e}(t_2)\boldsymbol{b}(t_2) + \boldsymbol{e}(t_1)\boldsymbol{b}(t_1)$$

$$= \underbrace{\boldsymbol{e}(t_2)\boldsymbol{SV}(t_2) - \boldsymbol{e}(t_1)\boldsymbol{SV}(t_1)}_{\textit{Satellite average Doppler}} - \underbrace{[\boldsymbol{e}(t_2) - \boldsymbol{e}(t_1)]\boldsymbol{b}(t_1)}_{\textit{relative LOS change}} - \boldsymbol{e}(t_2)\Delta\boldsymbol{b}$$

Satellite average Doppler and relative LOS change corrections are very sensitive to user position and satellite position error. Moreover, discussions on the impact of atmospheric delay, satellite clock bias and relativistic effect on time-differenced model can be found in [van Graas, et al., 2003]. In this paper, tropospheric delay was corrected using UNB3m model [Leandro, et al., 2006] and satellite clock was corrected using broadcast ephemeris. If broadcast ephemeris are used, special attention must be paid to epochs when ephemeris are updated. The same ephemeris has to be used for time t_1 and t_2.

B. APPENDIX: DOPPLER MULTIPATH FOR A UBLOX LEA-4T CONNECTED TO A PATCH ANTENNA

The patch antenna was on the top of the same vehicle, at a distance of 70 cm from the Novatel geodetic-grade antenna used in 4.1.
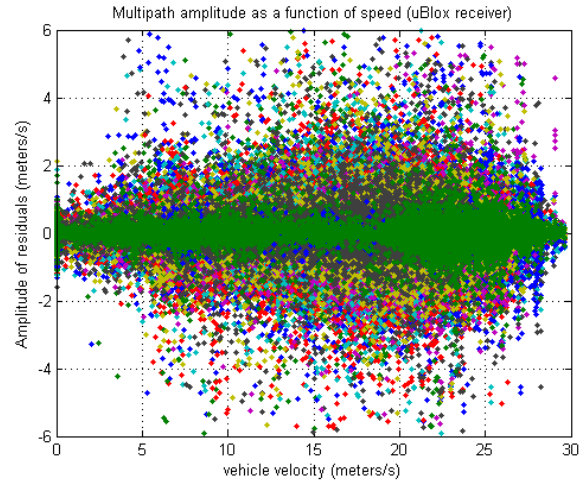

Figure 18 Doppler single-differenced multipath as a function of receiver velocity (uBlox receiver + patch antenna, 4Hz data collected on rural roads near Biscarosse and on Bordeaux's beltway, France)
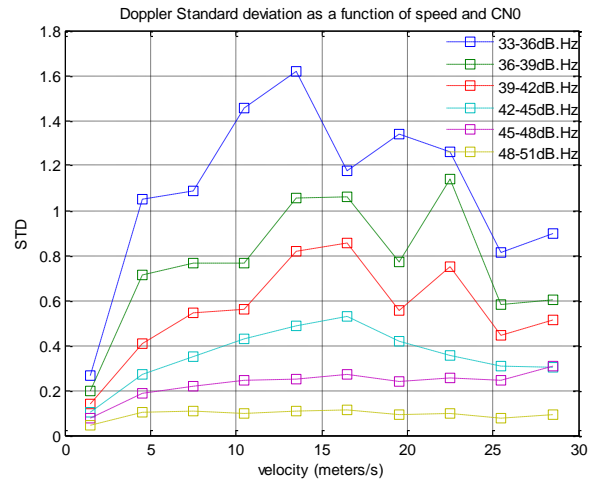

Figure 19 Estimated standard deviation of Doppler multipath on uBlox receiver + patch antenna, as a function of speed and C/N0. Standard deviation was estimated for speed "slices" of 3m.s-1, from 0 to 30 m.s-1
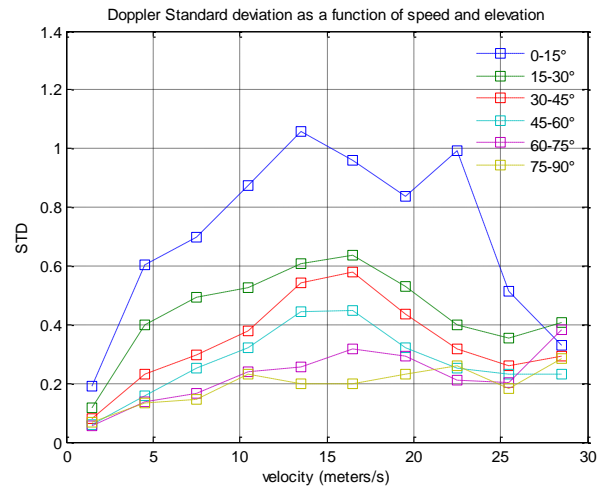

Figure 20 Estimated standard deviation of Doppler multipath on uBlox receiver + patch antenna, as a function of speed and

Results obtained are approximately 2.5 times less precise
than the one obtained with the Novatel receiver and 1.3
time less precise than the one obtained from the same
uBlox model plugged to a geodetic-grade antenna. Apart
from the Doppler weighting method proposed in 4.2, an
elevation mask of 15° is recommended as the amplitude
of multipath standard deviation dramatically increase for
very low-elevation satellite, as seen on Figure 20.